Optica Applicata, Vol. LV, No. 1, 2025
DOI: 10.37190/oa/200033

Digital image correlation (DIC) based stereo matching method for binocular structured light system (BSLS)

Wenjie Li[1,2,*], Beibei Wang[1], Yuyuan Huang[1], Yang Huang[1], Wenbin Huang[2], Haijian Wang[1]

[1]Guangxi Key Laboratory of Manufacturing System & Advanced Manufacturing Technology, School of Mechanical and Electrical Engineering, Guilin University of Electronic Technology, Guilin 541004, China

[2]Engineering Research Center of Digital Imaging and Display, Ministry of Education, Soochow University, Suzhou 215006, China

With the advantages of non-contact, quick and high accuracy, binocular stereo vision technology is popular in the fields of industrial inspection and measurement. To improve the result of stereo matching, phase consistency constrain based on the fringe projection profilometry (FPP) is performed. The phase unwrapping is generally employed to avoid the phase ambiguity, which is unrobust or time consuming. Aiming at this problem, a digital image correlation (DIC) assisted phase consistency method is proposed to achieve stereo matching with high accuracy, only three fringe patterns and one digital speckle pattern are needed. Two-step strategy is performed to get the homonymy points. The epipolar constraint and DIC algorithm can get the matching with pixel level, and then the wrapping consistency constraint is used to get a sub-pixel matching. To improve the matching accuracy, the Hilbert transform is employed to compensate the phase nonlinear error. As to the regions with low modulation, the disparity refinement algorithm based on neighboring disparity constrain is performed. The experiment results show that the reconstruction accuracy of proposed method is comparative with the multi-step phase shift plus multi-frequency heterodyne method.

Keywords: stereo matching, fringe projection profilometry, digital image correlation, Hilbert transformation.

1. Introduction

With advantages of high accuracy, high efficiency, and non-contact, binocular stereo vision technology is popular in the fields of industrial manufacturing, aerospace engineering and medical diagnosis. To overcome the influence of weak texture, structured - light-based stereo vision technologies have been extensively studied and utilized [1]. Among them, fringe projection profilometry (FPP) can perform 3D shape measurement with high accuracy and resolution benefitting from the characteristic of high spa-

tial resolution of sinusoidal phase encoding [2]. Compared to the Fourier transform profilometry (FTP) [3,4] in the FPP, the phase-shift profilometry (PSP) has been widely used in practical applications due to its greater robustness to phase noise induced by ambient illumination and surface reflectivity [5-8].

PSP generally uses *N*-step phase shift algorithm to compute the phase information ranging from $-\pi$ to π, which is wrapped phase. To remove the phase ambiguity, phase unwrapping is performed to obtain a full-field continuous phase distribution generally. Phase unwrapping methods mainly classify as spatial-based phase unwrapping methods [9] and temporal-based phase unwrapping methods [10]. The spatial phase unwrapping methods remove the phase discontinuities by checking the phase values of nearby pixels, which can only produce a relative phase map and will fail for isolated or abrupt surfaces. In temporal phase unwrapping methods, represented by Gray-code -assisted methods [11] and multi-frequency methods [12-14], absolute phase maps for arbitrary scenes are obtained using temporal information, demonstrating great performance. Nevertheless, these methods are constrained by the increased fringe patterns.

In order to make accurate 3D shape measurements of arbitrary surfaces with fewer projection patterns, digital image correlation (DIC) assisted fringe projection methods have been developed [15-17], which can be classified as digital speckle-embedded fringe projection [18-20] and digital speckle-separated fringe projection [21-24]. The digital speckle embedded fringe projection method typically involves encoding speckle patterns into the phase-shifted patterns to assist the absolute phase unwrapping [19,24] or stereo phase matching [21,22,25] using DIC technology, which can be minimum projection patterns. However, the crosstalk error between fringe images and speckle image will affect the reconstruction result. ZHANG *et al*. [26] generated the lookup table (LUT) between wrapped phase and height by embedding speckle image into the fringe patterns in the single camera-projector system. The height ambiguity was avoided theoretically combing the LUT and DIC, and only requires four speckle-embedded projection patterns. However, this approach needs capturing multiple reference planes at different heights, limiting the measurement range. Additionally, embedding speckle patterns in the fringe patterns can impact the phase quality of the final 3D surface measurement. Compared to speckle-embedded fringe projection method, speckle-separated fringe projection method respectively projects the patterns of wrapping phase calculation and DIC calculation, which can avoid the information crosstalk errors. AN and ZHANG [27] designed single camera and projector-based reconstruction system combining the binary image with the phase shifting method. It requires only projecting one additional pattern and does not rely on prior knowledge of object depth and geometric variations. However, suffered from different sensor sizes between the projectors and cameras, it is necessary to crop and down sample (or up sample) images from the projector or camera images before generating the disparity map, which is time consuming. Aiming at this problem, priori information strategy by projecting the binary random pattern to the reference plane was proposed in their next work [24]. The DIC calculation was operated between the speckle images captured at reference plane and measured object

plane, respectively, and the resolution of two speckle images is consistency. However, the accuracy of phase unwrapping based on the virtual reverse camera model may be affected by the nonlinearity of epipolar constraint. GAI *et al*. [21] got the initial matching based on the speckle DIC technique, and refined the initial matching using the wrapped phase information in the binocular stereo vision system. However, many candidate points are used to get the initial matching point in the DIC calculation, which is complex and time consuming. Combining three-step phase shifts with digital speckle patterns in the binocular system, FENG *et al*. [28] obtained the absolute phase unwrapping map by employing trifocal tensor constraints to reject wrong candidate points, while the effectiveness might be affected by the phase jump and phase error. HU *et al*. [23] filtered the candidate points by re-projecting constrains, and get the disparity and absolute phase maps. As the model between projector and camera is added, nonlinear errors of projector which will affect the reconstruction result.

In this paper, a DIC-assisted FPP will be proposed in the binocular stereo vision system. Only four patterns are projected to get stereo matching. The Hilbert transform is operated to compensate the phase nonlinear error [29]. Epipolar constraint, wrapping phase consistency constrains and DIC constrain are performed to obtain the disparity map with sub-pixel. Both the theory and experiment have verified the feasibility and superiority of proposed method. The remaining sections of this paper are as follows: Section 2 introduces the principle of the proposed method; Section 3 conducts experiment to verify the effectiveness, reliability, and universality of the proposed method; and Section 4 summarizes the paper.

2. Principle analysis

The framework of proposed method is shown in Fig. 1. After image capture by left and right cameras, epipolar rectification is performed. Then the wrapping phases are gotten using fringe images I_1–I_3. Wrapping phase compensation algorithm based on the Hilbert transformation is carried out to reduce the nonlinear errors. Two steps strategy is used to get the stereo matching with sub-pixel. The DIC calculation is used to get the coarse disparity map, and wrapping phase consistency constrains is used to get the sub-pixel disparity map. The candidate matching points of DIC calculation are extracted base on the wrapping phase consistency constrains. For the low modulation regions, neighboring disparity detection is performed. At last, the point cloud of measured object is reconstructed combining the system calibration parameters.

2.1. Wrapping phase calculation

With the advantages of high robustness and accuracy, the phase shifting fringe algorithm is adopted in this research. The minimum number of fringe patterns for successful pixel-wise phase information retrieval in the phase shifting fringe analysis is three. The intensity of fringe images can be mathematically described as

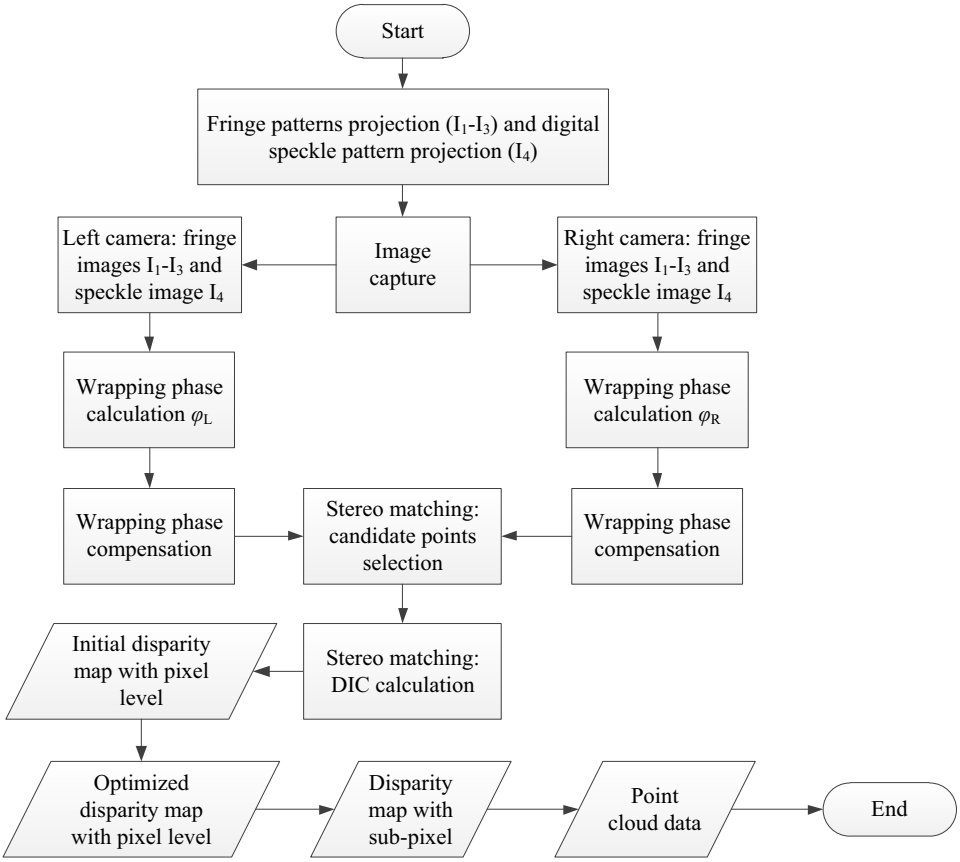

Fig. 1. Flowchart of proposed method.

$$\begin{cases} I_1(x,y) = A(x,y) + B(x,y)\cos\left[\varphi(x,y) - 2\pi/3\right] \\ I_2(x,y) = A(x,y) + B(x,y)\cos\left[\varphi(x,y)\right] \\ I_3(x,y) = A(x,y) + B(x,y)\cos\left[\varphi(x,y) + 2\pi/3\right] \end{cases} \tag{1}$$

where $A(x, y)$ is the background intensity, $B(x, y)$ is the modulation intensity, and (x, y) is the pixel coordinates. Wrapping phase value $\varphi(x, y)$ can be calculated by

$$\varphi(x,y) = \arctan\left\{\frac{\sqrt{3}\left[I_1(x,y) - I_3(x,y)\right]}{2I_2(x,y) - I_1(x,y) - I_3(x,y)}\right\} \tag{2}$$

Due to the arctangent function, the obtained phase value is wrapped within $[-\pi, \pi]$. With a discontinuity of $2n\pi$ (n is a non-zero integer), it is impossible to obtain homonymous point pairs by phase consistency when stereo matching is performed. The assisted constrain is needed to remove the phase ambiguity.

2.2. DIC-assisted stereo matching algorithm

For the stereo matching, it is necessary to remove the phase ambiguity when the phase consistency constrain is used to get the homonymy points. Generally, phase unwrapping technique is performed to remove phase ambiguity. However, the temporal phase unwrapping algorithm requires many projection patterns, while the spatial phase unwrapping algorithm is easily affected by the neighborhood phase involving the transmission of phase errors. So a DIC-assisted stereo matching algorithm is proposed in this paper, only one additional speckle pattern is projected to realize the point-by-point registration of the left and right cameras, which has the advantages of fast, accurate and robustness. The specific scheme is:

1) Epipolar rectification algorithm is used to ensure that the homonymous points is in the same line, and the time consuming of matching is reduced efficiently.

2) Candidate points extraction of stereo matching. Point (x, y) with a wrapping phase $\varphi_L(x, y)$ at left image can get sets of points at right image according to the threshold of wrapping phase consistency, which is 0.5.

3) Coarse disparity map generation. DIC algorithm is performed to all candidate points, and the period of matching point is confirmed according to the DIC scores.

4) Coarse disparity map optimization. For the regions of low modulation, some strategies are carried out to correct the matching point.

5) Fine disparity map generation. Based on the confirmed period and wrapping phase consistency, linear interpolation is chosen to get the matching with sub-pixel.

2.2.1. DIC-algorithm-assisted coarse disparity map generation

In this paper, DIC algorithm of digital speckle image is used to confirm the period or fringe order of matching point, and remove the ambiguity when the wrapping phase

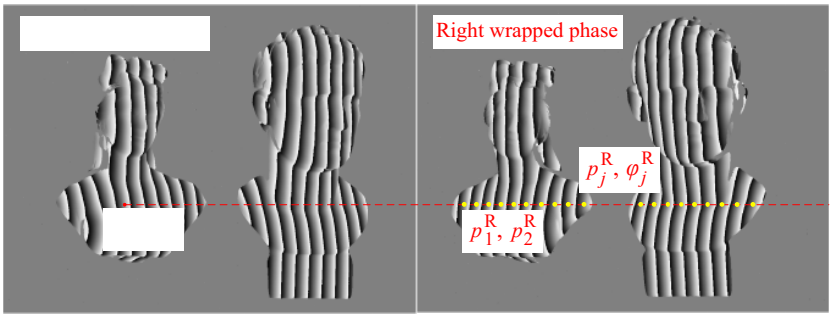

Fig. 2. Candidate matching points extraction.

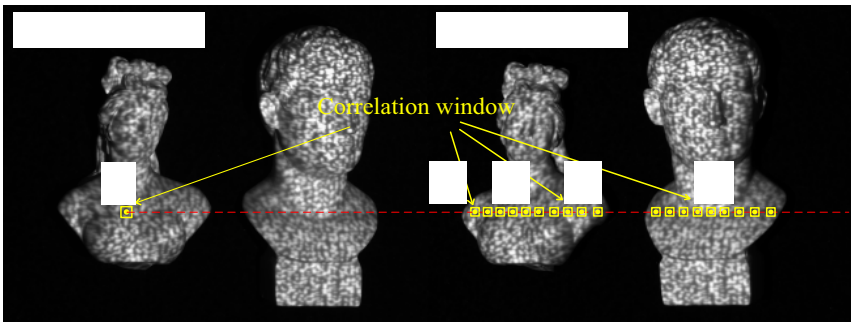

Fig. 3. DIC calculation of candidate points.

consistency is used as the matching condition. After the epipolar rectification, pixel p_i^{L} with phase value φ_i^{L} in the left wrapping phase map has the candidate points $M = \{ p_1^{\mathrm{R}}, p_2^{\mathrm{R}}, \ldots, p_j^{\mathrm{R}}, \ldots \}$ using the wrapping phase differences threshold, as shown in Fig. 2. A simple search strategy is proposed to obtain all candidate points by one traversal search. Each time when the absolute difference between left phase φ_i^{L} and right phase φ_j^{R} is lower than the threshold, the algorithm starts to locally track the wrapped phase value with minimum $\mathrm{abs}(\varphi_i^{\mathrm{L}} - \varphi_j^{\mathrm{R}})$ and record its disparity.

As shown in Fig. 3, DIC algorithm is used to confirm the matching point at the candidate points. To accelerate the calculation, variant of zero-mean normalized correlation coefficient (VZNCC) is used to calculate the scores of candidate points. The expression is as follows:

$$\mathrm{VZNCC} = \frac{n\sum_{i=1}^{n} I_i^{\mathrm{L}} I_i^{\mathrm{R}} - \left(\sum_{i=1}^{n} I_i^{\mathrm{L}}\right)\left(\sum_{i=1}^{n} I_i^{\mathrm{R}}\right)}{\sqrt{n\sum_{i=1}^{n} (I_i^{\mathrm{L}})^2 - \left(\sum_{i=1}^{n} I_i^{\mathrm{L}}\right)^2}\sqrt{n\sum_{i=1}^{n} (I_i^{\mathrm{R}})^2 - \left(\sum_{i=1}^{n} I_i^{\mathrm{R}}\right)^2}} \tag{3}$$

where n is the size of correlation window. I_i^{L} and I_i^{R} are the intensity of the pixels in the correlation window of the left and right speckle images. $\sum_{i=1}^{n} I_i^{\mathrm{L}}$, $\sum_{i=1}^{n} I_i^{\mathrm{R}}$, $\sum_{i=1}^{n} (I_i^{\mathrm{L}})^2$, and $\sum_{i=1}^{n} (I_i^{\mathrm{R}})^2$ can be obtained by the integral image technology, which greatly reduces the computational cost. The initial coarse disparity map can be generated by performing the above calculation on each pixel of the left image.

2.2.2. Coarse disparity map optimization

As to the complex measured object, the judgment of period order based on the DIC technology does not work to the region with low modulation. It is necessary to optimize the initial disparity map. The flowchart is shown in Fig. 4. The modulation map based

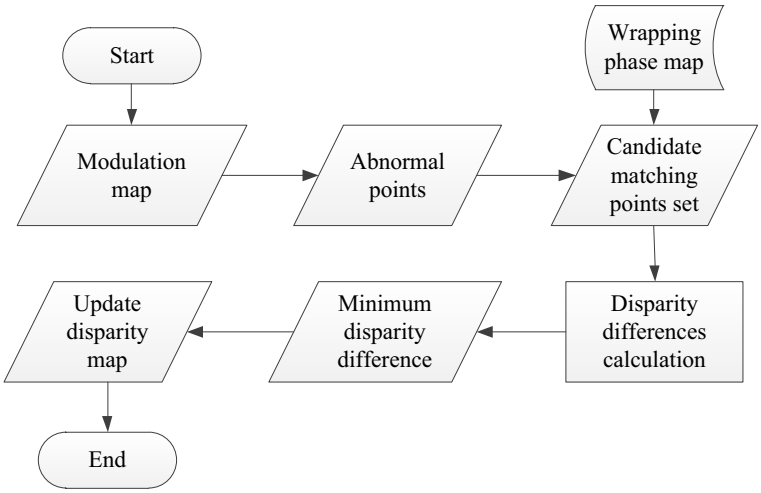

Fig. 4. Flowchart of disparity map optimization.

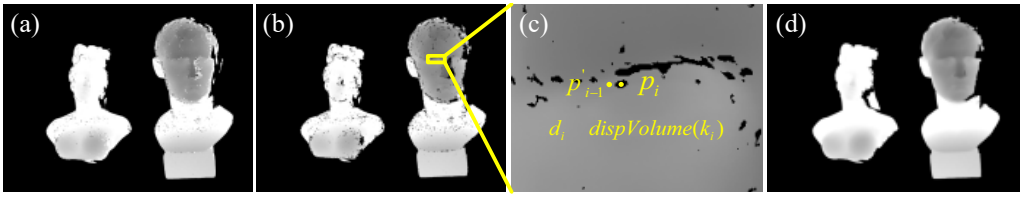

Fig. 5. Disparity map optimization. (a) Initial disparity map, (b) after removing the mismatched region, (c) partial enlarged detail, and (d) optimized disparity map.

on the fringe images is used to confirm the abnormal points, and the candidate matching points are extracted according to the wrapping phase consistency constrains described in Section 2.2.1. The minimum disparity difference between the candidate matching points p_i and nearest normal disparity point p_{i-1} is chosen as judging criteria of disparity update for the abnormal point. After the disparity update to the region with low modulation, noise point extraction is also performed, and linear interpolation is operated to correct the disparity of noise points. Figure 5 presents the result of disparity map optimization, which is effective and necessary.

2.2.3. Fine disparity map generation

In order to obtain the stereo matching with sub-pixel level, the wrapping phase is used as the constrain condition. To improve the matching accuracy, the phase nonlinear errors will be corrected by Hilbert transform at firstly. The phase errors at the spatial and Hilbert domains have the characteristic of same amplitude and opposite sign. So the mean of phases at the spatial and Hilbert domains is employed to compensate the phase nonlinear errors [29].

Theoretically, the image intensity of N-step PSP can be expressed as

$$I_n(x, y) = A(x, y) + B(x, y)\cos\left[\varphi(x, y) + \delta_n\right], \quad n = 1, 2, ..., N \tag{4}$$

where A and B represent the background and modulation intensity, respectively, and φ represents the phase information modulated by the object, $\delta_n = 2\pi(n-1)/N$ is the phase shift. In practical applications, the inherent nonlinear intensity response of the projector-camera device introduces high order harmonics into the fundamental harmonics of the fringe image, and the gamma distortion intensity can be expressed as

$$I_n^{\mathrm{C}} = (\alpha I_n)^{\gamma} = B_0 + \sum_{k=1}^{\infty} B_k \cos\left[k(\varphi + \delta_n)\right] = B_0 + \sum_{k=1}^{\infty} B_k \cos(k\varphi_n) \tag{5}$$

where α represents the surface reflectivity of the object, B_0 and B_k are the amplitudes of the DC component and the k-th harmonic component, respectively, φ_n represents the modulation phase, and γ is the gamma factor. Based on the least square algorithm (LSA), the modulation phase can be calculated as

$$\varphi = \arctan\left[\frac{-\sum_{n=1}^{N}(I_n \sin\delta_n)}{\sum_{n=1}^{N}(I_n \cos\delta_n)}\right] \tag{6}$$

The LSA phase based on gamma distortion is expressed as

$$\varphi^{\mathrm{C}} = \arctan\left[\frac{-\sum_{n=1}^{N}(I_n^{\mathrm{C}} \sin\delta_n)}{\sum_{n=1}^{N}(I_n^{\mathrm{C}} \cos\delta_n)}\right]$$

$$= \arctan\left\{\frac{-\sum_{n=1}^{N}\sum_{k=1}^{\infty}\left[B_k \cos(k\varphi_n)\sin\delta_n\right]}{\sum_{n=1}^{N}\sum_{k=1}^{\infty}\left[B_k \cos(k\varphi_n)\sin\delta_n\right]}\right\} \tag{7}$$

It can be deduced that the phase error model of PSP system can be simplified as

$$\Delta\varphi = \varphi^{\mathrm{C}} - \varphi = \arctan\left[\frac{-G_{N-1}\sin(N\varphi)}{1 + G_{N-1}\cos(N\varphi)}\right] \tag{8}$$

where G_s can be expressed as $G_s = \sum_{i=2}^{s}(\gamma - i + 1)/(\gamma + 1)$, the phase error model shows that the phase error is periodically distributed with respect to the phase φ.

The Hilbert transform (HT) of the phase shift image taken for the n-th time can be expressed as

$$I_n^{\mathrm{H}} = H[I_n] = -B\sin(\varphi + \delta_n) \tag{9}$$

where $H[\cdot]$ denotes an operator of HT. Due to the gamma effect, the intensity after Hilbert transform also has higher harmonics, which can be expressed as

$$I_n^{\mathrm{HC}} = -\sum_{k=1}^{\infty}\left[B_k \sin(k\varphi_n)\right] \tag{10}$$

The LSA-based phase in the HT domain can be expressed as

$$\varphi^{\mathrm{H}} = \arctan\left[\frac{\sum_{n=1}^{N}(I_n^{\mathrm{H}}\cos\delta_n)}{\sum_{n=1}^{N}(I_n^{\mathrm{H}}\sin\delta_n)}\right] \tag{11}$$

The phase of gamma distortion in HT domain is

$$\begin{aligned}\varphi^{\mathrm{HC}} &= \arctan\left[\frac{\sum_{n=1}^{N}(I_n^{\mathrm{HC}}\cos\delta_n)}{\sum_{n=1}^{N}(I_n^{\mathrm{HC}}\sin\delta_n)}\right] \\ &= \arctan\left\{\frac{\sum_{n=1}^{N}\sum_{k=1}^{\infty}\left[B_k\sin(k\varphi_n)\cos\delta_n\right]}{\sum_{n=1}^{N}\sum_{k=1}^{\infty}\left[B_k\sin(k\varphi_n)\sin\delta_n\right]}\right\}\end{aligned} \tag{12}$$

Similarly, the phase error model simplification of the PSP system in the HT domain can be derived as [29]:

$$\Delta\varphi^{\mathrm{H}} = \varphi^{\mathrm{HC}} - \varphi = \arctan\left[\frac{G_{N-1}\sin(N\varphi)}{1 - G_{N-1}\cos(N\varphi)}\right] \tag{13}$$

Equation (8) and Eq. (13) reveal that the phase error in the spatial and HT domain is a trigonometric function of the phase φ. The period is $T = 2\pi/N$, and the maximum phase error can be expressed as

$$\begin{cases} A_{\Delta\varphi} = |\Delta\varphi|_{\max} = \arcsin(|G_{N-1}|) \\ A_{\Delta\varphi}^{\mathrm{H}} = |\Delta\varphi^{\mathrm{H}}|_{\max} = \arcsin(|G_{N-1}|) \end{cases} \tag{14}$$

In addition, it can also be deduced that

$$\Delta\varphi^{\mathrm{H}}\Big|_{\varphi+\frac{T}{2}} = \arctan\left\{\frac{G_{N-1}\sin\left[N\left(\varphi+\frac{\pi}{N}\right)\right]}{1-G_{N-1}\cos\left[N\left(\varphi+\frac{\pi}{N}\right)\right]}\right\}$$

$$= \arctan\left[\frac{-G_{N-1}\sin(N\varphi)}{1+G_{N-1}\cos(N\varphi)}\right] = \Delta\varphi\big|_{\varphi} \tag{15}$$

It can be concluded that the characteristics of the periodic phase error distribution in these two domains are: (1) the same period $T = 2\pi/N$; (2) the same amplitude $A = \arcsin(|G_{N-1}|)$; (3) the distribution is a half-period shift, as shown in Eq. (15), resulting in the opposite distribution trend. Therefore, the average phase $\varphi^{\mathrm{M}} = (\varphi^{\mathrm{C}} + \varphi^{\mathrm{HC}})/2$ can be used as the corrected phase. Combining Eq. (8) and Eq. (13), the phase error of φ^{M} can be obtained as

$$\Delta\varphi^{\mathrm{M}} = \varphi^{\mathrm{M}} - \varphi = \frac{1}{2}(\Delta\varphi + \Delta\varphi^{\mathrm{H}}) = \frac{1}{2}\arctan\left[\frac{G_{N-1}^2\sin(2N\varphi)}{1-G_{N-1}^2\cos(2N\varphi)}\right] \tag{16}$$

The maximum phase error of the average phase is

$$\Delta\varphi^{\mathrm{M}}\big|_{\max} = \frac{1}{2}\arcsin(G_{N-1}^2) \tag{17}$$

The ratio of the maximum phase error after and before compensation is approximately:

$$r_{\Delta\varphi} = \frac{|\Delta\varphi^{\mathrm{M}}|_{\max}}{|\Delta\varphi|_{\max}} \approx \frac{\frac{1}{2}G_{N-1}^2}{|G_{N-1}|} = \frac{|G_{N-1}|}{2} \tag{18}$$

It can be seen that the maximum phase error is reduced to $|G_{N-1}|/2$ times after average processing. The specific steps of the proposed phase compensation method can be summarized as follows:

1) HT operation is performed to the fringe images, and the images in the Hilbert domain are gotten.

2) Wrapping phases calculation using the images at spatial and Hilbert domains, respectively.

3) Averaging the wrapping phase maps above.

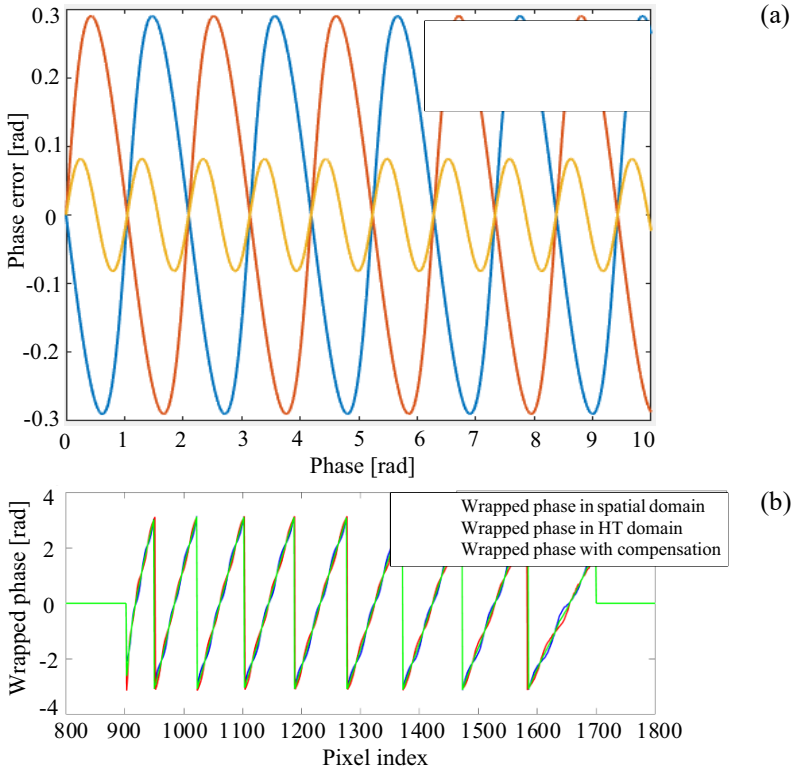

Fig. 6. Characteristics of phase error distribution. (a) The phase error with respect to phase, and (b) wrapped phase error correction.

To illustrate these characteristics, we created some phase error curves in the two domains through Eq. (8) and (13) with the parameters of $G_{N-1} = 0.4$ and $N = 3$, as demonstrated in Fig. 6(a). It is clearly shown that the above stated characteristics are correct, and the values of phase error in the two domains are approximately identical in magnitude and opposite in sign. In practical measurements, the Hilbert transform is used to correct the phase error of the wrapping phase of the object, as shown in Fig. 6(b).

After phase nonlinear error correction, the wrapping phase consistency is used for the fine matching with sub-pixel. As shown in Fig. 7, the wrapping phases of homonym points $p_{\mathrm{L}}(u_{\mathrm{l}}, v)$ and $p_{\mathrm{R}}(u_{\mathrm{r}}, v)$ are respectively $\varphi_{\mathrm{l}}(u_{\mathrm{l}}, v)$ and $\varphi_{\mathrm{r}}(u_{\mathrm{r}}, v)$. The linear interpolation algorithm is performed to get the sub-pixel coordinate.

$$u = \begin{cases} u_{\mathrm{r}} + \dfrac{\varphi_{\mathrm{l}}(u_{\mathrm{l}}, v) - \varphi_{\mathrm{r}}(u_{\mathrm{r}}, v)}{\varphi_{\mathrm{r}}(u_{\mathrm{r}} + 1, v) - \varphi_{\mathrm{r}}(u_{\mathrm{r}}, v)} & \text{if} \quad \varphi_{\mathrm{l}}(u_{\mathrm{l}}, v) > \varphi_{\mathrm{r}}(u_{\mathrm{r}}, v) \\ u_{\mathrm{r}} - \dfrac{\varphi_{\mathrm{r}}(u_{\mathrm{r}}, v) - \varphi_{\mathrm{l}}(u_{\mathrm{l}}, v)}{\varphi_{\mathrm{r}}(u_{\mathrm{r}}, v) - \varphi_{\mathrm{r}}(u_{\mathrm{r}} - 1, v)} & \text{if} \quad \varphi_{\mathrm{l}}(u_{\mathrm{l}}, v) \le \varphi_{\mathrm{r}}(u_{\mathrm{r}}, v) \end{cases} \tag{19}$$

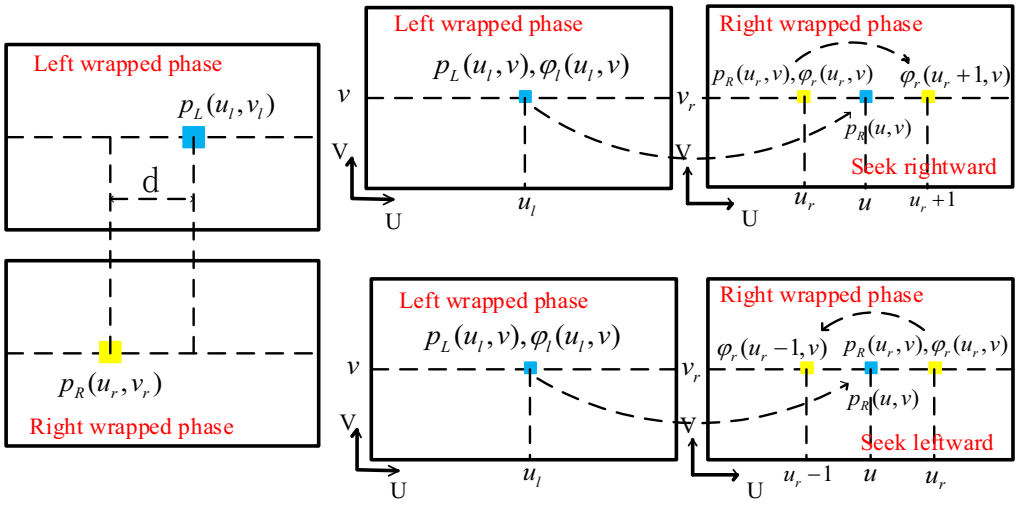

Fig. 7. Fine matching with sub-pixel.

When the initial matching point is at the periodic edge, the phase difference of neighboring points may be large, as shown in Fig. 8. At this situation, the period correction is necessary. If $\varphi_l(u_l, v) > \varphi_r(u_r, v)$, search along right side will be operated. When point (u_r, v) locates the maximum phase of a period, the phase of point $(u_r + 1, v)$ will jump. So the phase of point $(u_r + 1, v)$ should compensate 2π before the phase interpolation, as shown in Fig. 8. Similarly, if $\varphi_l(u_l, v) < \varphi_r(u_r, v)$, search along left side will be operated. When point (u_r, v) locates the minimum phase of a period, the phase of point $(u_r - 1, v)$ should reduce 2π before the phase interpolation.

After refinement, the final refined disparity map with sub-pixel level can be obtained. Finally, the point cloud data is obtained combining the system calibration parameters.

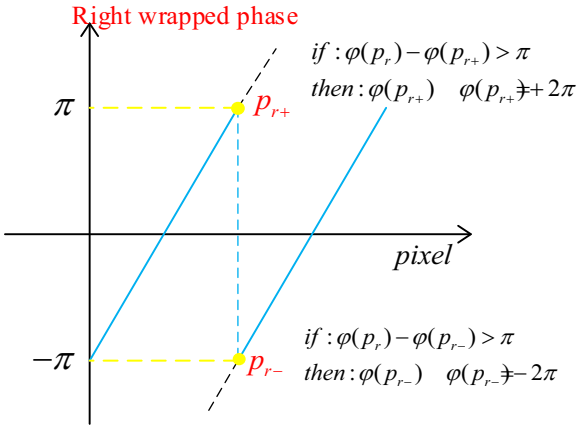

Fig. 8. Special case of sub-pixel matching.

3. Experiment analysis and discussion

To verify the feasibility of proposed method, a structured projection-assisted stereo vision system composed of two industrial cameras and one digital light projector (DLP) is designed, as shown in Fig. 9. The resolutions of cameras and DLP are 2592×1944 pixels and 912×1140 pixels, respectively. System calibration is operated to get the relationship between two cameras.

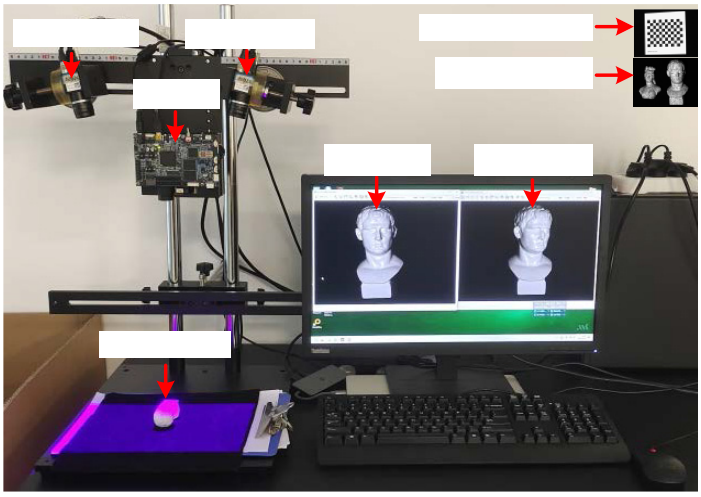

Fig. 9. Experiment device.

To verify the feasibility of the proposed method, three standard objects are chosen as the measured objects, including checkerboard calibration plate, step block and ceramic ball. The reconstruction result of three frequencies heterodyne algorithm with 12-step phase-shifting is chosen as the ideal result, and the reconstruction result of DIC-assisted matching algorithm with 3-step phase-shifting is chosen as compared group to verify the necessary of phase nonlinear error compensation.

Figure 10 shows the reconstruction result of the checkerboards. Plane fitting is operated based on the random sampling consensus (RANSAC) algorithm [30]. Flatness F is defined as the root mean square error (RMSE) of point cloud to the fitted plane. The expression is:

$$F = \sqrt{\frac{1}{n}\sum_{i=1}^{n} d_i^2} \tag{20}$$

where d_i is the distance from the point cloud to the fitted plane, and n is the number of point cloud. The flatness comparison using different methods is shown in Table 1. It implies that the proposed method can get a high accuracy result, and the phase nonlinear compensation is necessary when few fringe patterns are used to calculate the wrapping phase.

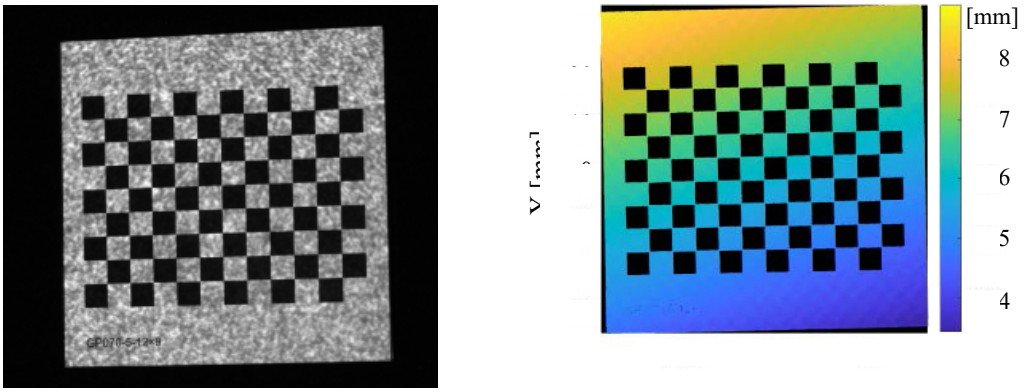

(a) (b)

Fig. 10. Reconstruction of checkerboard calibration plate. (a) Speckle image, and (b) 3D point cloud.

T a b l e 1. Reconstruction result comparison of checkerboard.

Experimental methods	Flatness [mm]
3-step phase shift and DIC-assisted matching	0.0512
12-step phase shift and 3 frequencies	0.0271
Proposed method	0.0281

Figure 11 and Table 2 present the measurement results of step block. It also can be seen that proposed method reconstructed the step block efficiently. The measurement results of step distances approach the multi-frequency with multi-step phase shift algorithm, while only four patterns are needed, which is quick and highly accurate.

To verify the feasibility and high accuracy of proposed method, the reconstruction of the standard ceramic ball is performed. The information of the standard ceramic ball is as follows. Company: Nanchang Dingsheng Automation Technology Co., Ltd., type: DS-MCB-D38.1GZ, diameter: 38.0845 mm, and roundness: 0.0016 mm.

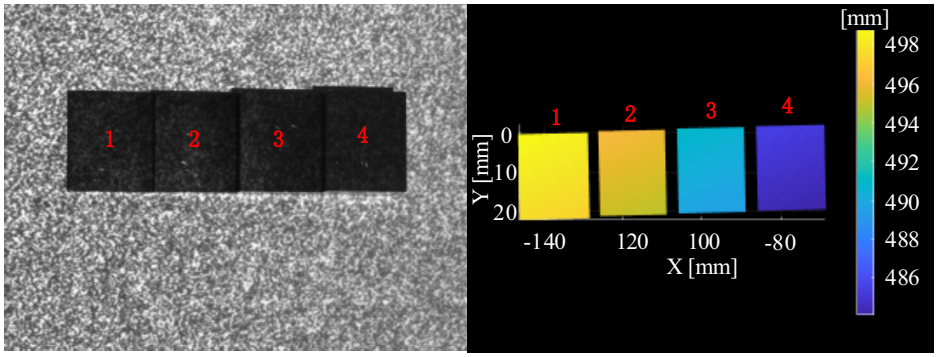

(a) (b)

Fig. 11. Reconstruction result of step block. (a) Speckle image, and (b) 3D point cloud.

T a b l e 2. Measurement result of step block.

	Ideal value [mm]	Measured distance [mm]		Absolute error [mm]	
		12-step phase shift and 3-frequency	Proposed method	12-step phase shift and 3-frequency	Proposed method
Step 1~2	2.0000	1.9846	1.9787	0.0154	0.0213
Step 2~3	5.0000	5.0124	5.0147	0.0124	0.0147
Step 3~4	5.0000	4.9715	4.9720	0.0285	0.0280

Figure 12 and Table 3 show the measurement result comparisons of different methods. As presented in Fig. 12 (c), the measured profile of sphere surface is smooth using the proposed method, which is near the result of multi-step phase shift and multi-frequency algorithm. The result in Table 3 also verified the feasibility and superiority of proposed method. In the measurement of diameter, the measurement error is 0.0089 mm

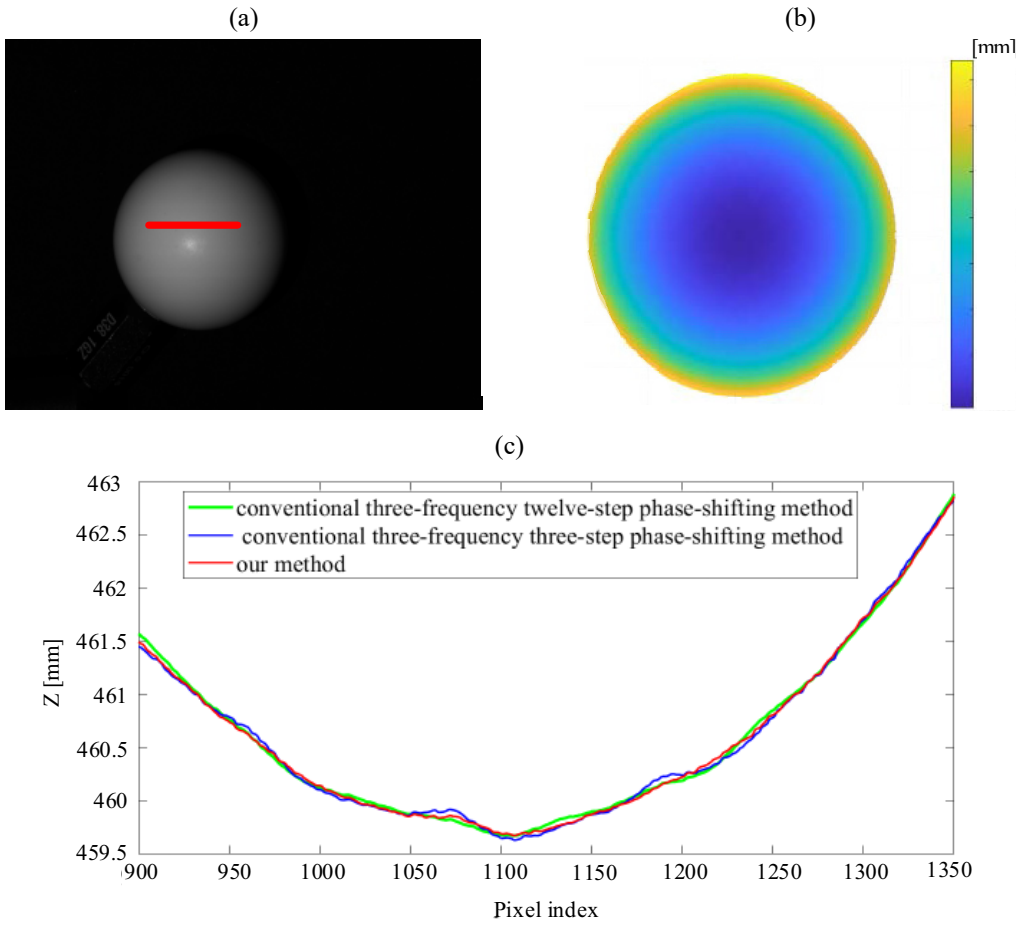

Fig. 12. Measurement results of ceramic ball. (a) Ceramic ball image, (b) 3D point cloud, and (c) 3D shape comparison of multi-frequency heterodyne method and proposed method.

T a b l e 3. Measurement result comparison of ceramic ball.

Experimental methods	Diameter [mm]	Absolute deviation [mm]
3-step phase shift and DIC-assisted matching	38.0405	0.044
12-step phase shift and 3 frequencies	38.0756	–0.0089
Proposed method	38.0934	0.0089

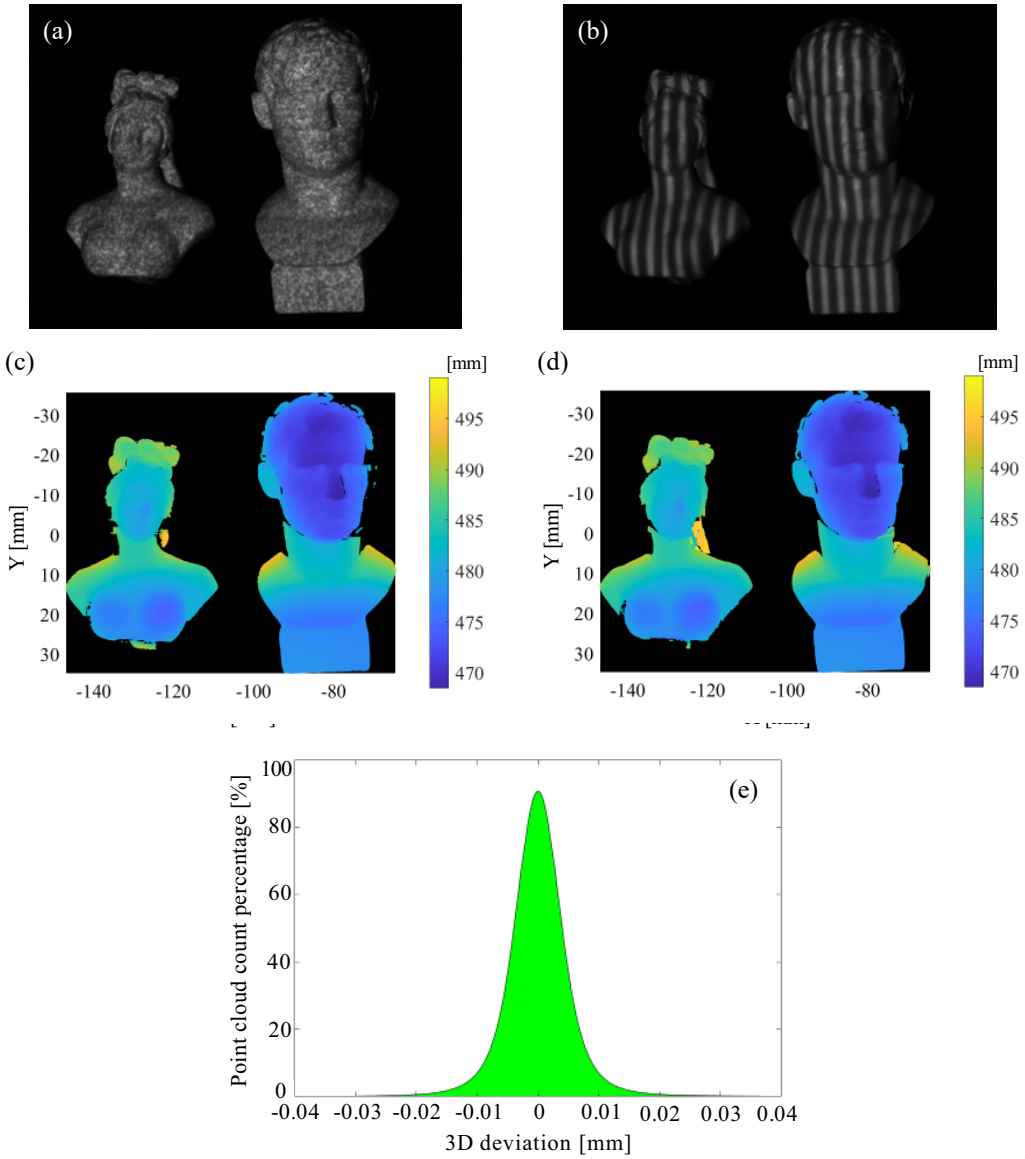

Fig. 13. Measurement comparison of complex object. (a) Digital speckle images and (b) fringe image from left and right cameras. The reconstruction results using (c) multi-step plus multi-frequency algorithm and (d) proposed method. (e) 3D deviation statistics of two methods.

using the proposed method, which improves 79.7% compared with the three-step phase shift and multi-frequency method.

Figure 13 presents the result comparison of complex objects with two isolated surfaces, using the multi-step phase shift plus multi-frequency heterodyne method and proposed method. The number of point cloud is 1 488 840, and the distance deviation of two methods within 0.01 mm is 1 371 875, which is about 92.14%, which implies the feasibility of proposed method. The experiments above all show that the reconstruction result of proposed method is comparative with the multi-step phase shift plus multi-frequency heterodyne method, while only four projection patterns are needed, which is feasible and superior.

4. Conclusion and discussion

In this paper, a DIC-assisted stereo matching method is proposed in the 3D measurement. Only four projection patterns are needed to get the disparity map with sub-pixel level. Combining the epipolar constraint, wrapping phase consistency constrains and DIC constrain, the homonymy points are gotten by pixel-wise, which is robust. Different from traditional unwrapping phase consistency constrains, the wrapping phase is not unwrapped, which is time-saving. The Hilbert transformation is performed to improve the phase nonlinear error when few fringe patterns are used to get the wrapping phase. To the regions with low modulation, the strategy of neighboring disparity detection is operated, and the period order is corrected. The experiment results show that the reconstruction results of proposed method are comparative with the multi-step phase shift plus multi-frequency heterodyne method, which is feasible and superior.

In this paper, the DIC-assisted stereo matching method is to determine the fringe order K of each pixel-by-pixel DIC calculation, which is still relatively time-consuming. And in the binocular system, there are still problems of missing and empty 3D reconstruction point cloud data due to the difference in the field of view of the left and right cameras. Therefore, in the monocular system, using only a few candidate points to determine the fringe order of all pixels in each fringe period to reduce the computational cost will be our next interesting work.

Acknowledgement

This work was financially supported by Guangxi Natural Sciense Foundation (Grant No. 2025GXNSFAA069774), Guangxi Key Laboratory of Manufacturing System & Advanced Manufacturing Technology (Grant No. AD25069080), Engineering Research Center of Digital Imaging and Display, Ministry of Education, Soochow University (Grant No. SDGc2319).

Reference

[1] Yang S., Wu G., Wu Y., Yan J., Luo H., Zhang Y., Liu F., *High-accuracy high-speed unconstrained fringe projection profilometry of 3D measurement*, Optics & Laser Technology **125**, 2020: 106063. https://doi.org/10.1016/j.optlastec.2020.106063

[2] Zhang S., *Absolute phase retrieval methods for digital fringe projection profilometry: A review*, Optics and Lasers in Engineering **107**, 2018: 28-37. https://doi.org/10.1016/j.optlaseng.2018.03.003

[3] ZHANG H., ZHANG Q., LI Y., LIU Y., *High speed 3D shape measurement with temporal Fourier transform profilometry*, Applied Sciences **9**(19), 2019: 4123. https://doi.org/10.3390/app9194123
[4] ZHANG S., *Comparing Hilbert transform profilometry and Fourier transform profilometry (Conference Presentation)*, Proceedings of the SPIE, Vol. 10991, Dimensional Optical Metrology and Inspection for Practical Applications VIII, 2019: 1099107. https://doi.org/10.1117/12.2517870
[5] ZUO C., FENG S., HUANG L., TAO T., YIN W., CHEN Q., *Phase shifting algorithms for fringe projection profilometry: A review*, Optics and Lasers in Engineering **109**, 2018: 23-59. https://doi.org/10.1016/j.optlaseng.2018.04.019
[6] YUAN H., LI Y., ZHAO J., ZHANG L., LI W., HUANG Y., GAO X., XIE Q., *An adaptive fringe projection method for 3D measurement with high-reflective surfaces*, Optics & Laser Technology **170** 2024: 110062. https://doi.org/10.1016/j.optlastec.2023.110062
[7] XU J., ZHANG S., *Status, challenges, and future perspectives of fringe projection profilometry*, Optics and Lasers in Engineering **135**, 2020: 106193. https://doi.org/10.1016/j.optlaseng.2020.106193
[8] WU K., LI M., LU L., XI J., *Reconstruction of isolated moving objects by motion-induced phase shift based on PSP*, Applied Sciences **12**(1), 2022: 252. https://doi.org/10.3390/app12010252
[9] SU X., CHEN W., *Reliability-guided phase unwrapping algorithm: A review*, Optics and Lasers in Engineering **42**(3), 2004: 245-261. https://doi.org/10.1016/j.optlaseng.2003.11.002
[10] HE X., KEMAO Q., *A comparative study on temporal phase unwrapping methods in high-speed fringe projection profilometry*, Optics and Lasers in Engineering **142**, 2021: 106613. https://doi.org/10.1016/j.optlaseng.2021.106613
[11] WU Z., GUO W., LI Y., LIU Y., ZHANG Q., *High-speed and high-efficiency three-dimensional shape measurement based on Gray-coded light*, Photonics Research **8**(6), 2020: 819-829. https://doi.org/10.1364/PRJ.389076
[12] TOWERS C.E., TOWERS D.P., JONES J.D.C., *Absolute fringe order calculation using optimised multi-frequency selection in full-field profilometry*, Optics and Lasers in Engineering **43**(7), 2005: 788-800. https://doi.org/10.1016/j.optlaseng.2004.08.005
[13] MA Z., LU Z., LI Y., DAI Y., *Multi-frequency fringe projection profilometry: Phase error suppression based on cycle count adjustment*, Applied Sciences **13**(8), 2023: 5117. https://doi.org/10.3390/app13085117
[14] LIU J., SHAN S., XU P., ZHANG W., LI Z., WANG J., XIE J., *Improved two-frequency temporal phase unwrapping method in fringe projection profilometry*, Applied Physics B **130**, 2024: 42. https://doi.org/10.1007/s00340-024-08183-3
[15] ZHOU Y., SUN C., CHEN J., *Adaptive subset offset for systematic error reduction in incremental digital image correlation*, Optics and Lasers in Engineering **55**, 2014: 5-11. https://doi.org/10.1016/j.optlaseng.2013.10.014
[16] LIN Y., HUANG P., NI Z., XIE S., BAI Y., DONG B., *Full-field vibration measurements by using high -speed two-dimensional digital image correlation*, Applied Sciences **13**(7), 2023: 4257. https://doi.org/10.3390/app13074257
[17] HAGARA M., HUŇADY R., LENGVARSKÝ P., VOCETKA M., PALIČKA P., *The calibration process and setting of image brightness to achieve optimum strain measurement accuracy using stereo-camera digital image correlation*, Applied Sciences **13**(17), 2023: 9512. https://doi.org/10.3390/app13179512
[18] LOHRY W., CHEN V., ZHANG S., *Absolute three-dimensional shape measurement using coded fringe patterns without phase unwrapping or projector calibration*, Optics Express **22**(2), 2014: 1287-1301. https://doi.org/10.1364/OE.22.001287
[19] YIN W., FENG S., TAO T., HUANG L., TRUSIAK M., CHEN Q., ZUO C., *High-speed 3D shape measurement using the optimized composite fringe patterns and stereo-assisted structured light system*, Optics Express **27**(3), 2019: 2411-2431. https://doi.org/10.1364/OE.27.002411
[20] DENG H., LING X., WANG Y., YAO P., MA M., ZHONG X., *High-speed and high-accuracy fringe projection profilometry without phase unwrapping*, Optics and Lasers in Engineering **140**, 2021: 106518. https://doi.org/10.1016/j.optlaseng.2020.106518

[21] Gai S., Da F., Dai X., *Novel 3D measurement system based on speckle and fringe pattern projection*, Optics Express **24**(16), 2016: 17686-17697. https://doi.org/10.1364/OE.24.017686

[22] Fu K., Xie Y., Jing H., Zhu J., *Fast spatial–temporal stereo matching for 3D face reconstruction under speckle pattern projection*, Image and Vision Computing **85**, 2019: 36-45. https://doi.org/10.1016/j.imavis.2019.02.007

[23] Hu P., Yang S., Zhang G., Deng H., *High-speed and accurate 3D shape measurement using DIC-assisted phase matching and triple-scanning*, Optics and Lasers in Engineering **147**, 2021: 106725. https://doi.org/10.1016/j.optlaseng.2021.106725

[24] Liao Y.H., Xu M., Zhang S., *Digital image correlation assisted absolute phase unwrapping*, Optics Express **30**(18), 2022: 33022-33034. https://doi.org/10.1364/OE.470704

[25] Zhong K., Li Z., Shi Y., Wang C., Lei Y., *Fast phase measurement profilometry for arbitrary shape objects without phase unwrapping*, Optics and Lasers in Engineering **51**(11), 2013: 1213-1222. https://doi.org/10.1016/j.optlaseng.2013.04.016

[26] Zhang J., Guo W., Wu Z., Zhang Q., *Three-dimensional shape measurement based on speckle-embedded fringe patterns and wrapped phase-to-height lookup table*, Optical Review **28**, 2021: 227-238. https://doi.org/10.1007/s10043-021-00653-9

[27] An Y., Zhang S., *Three-dimensional absolute shape measurement by combining binary statistical pattern matching with phase-shifting methods*, Applied Optics **56**(19), 2017: 5418-5426. https://doi.org/10.1364/AO.56.005418

[28] Feng S., Chen Q., Zuo C., Asundi A., *Fast three-dimensional measurements for dynamic scenes with shiny surfaces*, Optics Communications **382**, 2017: 18-27. https://doi.org/10.1016/j.optcom.2016.07.057

[29] Cai Z., Liu X., Jiang H., He D., Peng X., Huang S., Zhang Z., *Flexible phase error compensation based on Hilbert transform in phase shifting profilometry*, Optics Express **23**(19), 2015: 25171-25181. https://doi.org/10.1364/OE.23.025171

[30] Li W., Zhang Z., Jiang Z., Gao X., Tan Z., Wang H., *A RANSAC based phase noise filtering method for the camera-projector calibration system*, Optoelectronics Letters **18**, 2022: 618-622. https://doi.org/10.1007/s11801-022-2045-2

Received December 23, 2024
in revised form January 10, 2025